RESEARCH PAPER

Formulation, Optimization and Evaluation of Telmisartan Nanosuspension by High-Pressure Homogenization Using a Central Composite Design

Himanshu[1*], Seema1, Anuj Mittal[1], Preeti Kuniyal[1], Bharat Bhushan[2], Satyender Kumar[2]

[1]*Department of Pharmaceutical, HIMT College of Pharmacy, Greater Noida, U.P*
[2]*R&D Head, Cuckos Pharmaceutical Pvt. Ltd., Sampla, Haryana*
[2]*School of Pharmacy, Sharda University, Greater Noida, U.P*
[*]***Corresponding author:*** *himanshuparasharonline@gmail.com*

Received: 14th June, 2026; Revised: 20th July 2026; Accepted: 26th October 2026; Available Online: 28th October 2026

ABSTRACT

Telmisartan is a first-line angiotensin II receptor blocker that belongs to BCS Class II, and its oral absorption is limited by its very low and pH-dependent aqueous solubility. The present work aimed to formulate and evaluate a nanosuspension of telmisartan by the top-down high-pressure homogenization (HPH) technique, using Tween 80 and lecithin as stabilizers and PEG 400 as a wetting agent, so as to enhance its saturation solubility and dissolution rate. After preformulation studies (solubility, melting point, FTIR, DSC, PXRD, drug–excipient compatibility and a validated UV method at 296 nm), the effects of lecithin concentration (X1), Tween 80 concentration (X2) and homogenization pressure (X3) were optimized by a three-factor, five-level, 20-run central composite design (CCD), with particle size, polydispersity index (PDI), absolute zeta potential and drug release at 15 min (Q15) as responses. Quadratic models were significant for all responses ($R^2 > 0.98$) with non-significant lack of fit. The optimized formulation (0.44% w/v lecithin, 0.70% w/v Tween 80, 1240 bar, 10 cycles; overall desirability 0.872) had a particle size of 248.8 ± 4.9 nm, a PDI of 0.256 ± 0.004, a zeta potential of −27.0 ± 0.5 mV and a drug content of 99.4 ± 0.7%, and the prediction errors were within ±1.5%. The crystalline form of the drug was retained, and the saturation solubility increased 6.1-fold in water and 5.5-fold in phosphate buffer pH 7.5. In pH 7.5 buffer, 82.2% of the drug was released in 15 min from the nanosuspension, against 14.6% from the pure drug (dissolution efficiency 89.6% vs. 30.3%), and the release followed the Korsmeyer–Peppas model (n = 0.564). The nanosuspension was stable for 3 months at 5 ± 3 °C and 25 ± 2 °C/60 ± 5% RH and remained within the acceptance limits under accelerated conditions. HPH with a Tween 80–lecithin stabilizer system is therefore a promising approach to overcome the dissolution-limited absorption of telmisartan.

Keywords: Telmisartan; nanosuspension; high-pressure homogenization; central composite design; Tween 80; lecithin; dissolution; stability

How to cite this article: Himanshu, Seema, Mittal A, Kuniyal P, Bhushan B, Kumar S, Formulation, Optimization and Evaluation of Telmisartan Nanosuspension by High-Pressure Homogenization Using a Central Composite Design. Int J Drug Deliv Technol. 2026;16(89s): 663-676; DOI: 10.25258/ijddt.16.89s.72
Source of support: Nil.
Conflict of interest: None

1. INTRODUCTION

Hypertension, defined as a persistent elevation of arterial blood pressure, is one of the most common chronic non-communicable conditions worldwide and the single largest modifiable risk factor for cardiovascular disease, stroke, chronic kidney disease and premature death[1,2]. The number of adults aged 30–79 years living with hypertension has roughly doubled over three decades to about 1.28 billion in 2019, nearly half of the affected adults are unaware of their condition, and only about one in five has blood pressure under control[3]. India carries a particularly heavy burden, with estimates of the prevalence of hypertension ranging from nearly 30% in a meta-analysis of Indian studies to approximately 35% in the ICMR-INDIAB national study, and with low levels of awareness, treatment and control[4,5]. In addition to access to care, the availability of effective, well-absorbed and affordable antihypertensive formulations therefore remains an important determinant of population-level blood pressure control.

Telmisartan is a non-peptide angiotensin II type 1 (AT1) receptor blocker that binds with high affinity and long dissociation half-time to the AT1 receptor and acts as an insurmountable antagonist; in addition, it is a partial agonist of PPAR-γ, which may confer favourable metabolic effects[6–8]. In the ONTARGET trial it was as effective as ramipril in reducing cardiovascular events in high-risk patients and was better tolerated[9]. After oral administration telmisartan is absorbed rapidly, with peak plasma concentrations within 0.5–1.5 h, but its absolute bioavailability is dose-dependent, rising from about 42% after a 40 mg dose to about 58% after 160 mg[10,11]. As a BCS Class II drug, it permeates the intestinal epithelium readily but dissolves slowly in the gastrointestinal fluids within the limited transit time, so that its absorption is dissolution rate-limited, which results in incomplete and variable bioavailability[6]. Several approaches have been explored to improve the dissolution

**Author for Correspondence: himanshuparasharonline@gmail.com*

and bioavailability of telmisartan, including pH-modulated solid dispersions[12], supersaturable self-microemulsifying systems[13] and drug nanoparticles prepared by media milling[14]. Most of these approaches carry limitations such as physical instability, high excipient content or complex equipment. Reduction of the particle size of the drug to the nanometre range, formulated as a stabilized nanosuspension, is a rational alternative. A nanosuspension is a biphasic system of pure, poorly water-soluble drug particles dispersed in an aqueous vehicle and stabilized by surfactants and/or polymers, with a mean particle size below 1 μm[15,16]; because the drug itself constitutes the particle, the drug loading is close to 100% and no matrix material is needed[17]. Nanosizing increases the specific surface area in inverse proportion to the particle diameter, and thereby accelerates dissolution according to the Noyes–Whitney equation, while the highly curved surface of nanoparticles also raises the saturation solubility (Ostwald–Freundlich and Kelvin relationships)[17–19].

High-pressure homogenization is a “top-down” technique in which a coarse drug suspension is forced under high pressure through a very narrow homogenizing gap; cavitation, shear and impact forces fracture the drug crystals down to the nanometre size range[17,20]. The technique is scalable, avoids organic solvents, gives narrow particle size distributions and is already used for marketed nanocrystal products[21]. The literature shows that nanosizing of telmisartan by antisolvent precipitation and media milling has given large improvements in solubility, dissolution and bioavailability, but the application of HPH to telmisartan, with systematic optimization of the formulation and process variables and with evaluation of dissolution and stability, has not been investigated in depth.

The aim of the present work was therefore to formulate and evaluate a nanosuspension of telmisartan, a poorly water-soluble BCS Class II antihypertensive drug, using the top-down HPH technique, so as to enhance its saturation solubility and dissolution rate and to obtain a stable nanosuspension that can serve as a platform for improved oral delivery. The formulation and process variables were optimized by a statistical design of experiments, and the optimized product was characterized for particle size, zeta potential, solid-state properties, saturation solubility, dissolution behaviour and physical stability.

2. MATERIALS AND METHODS

2.1 Materials and equipment

The pure drug sample of telmisartan was obtained as a gift sample from Cuckos Pharmaceutical Pvt. Ltd., Sampla, Haryana, India, and was used as received. Tween 80 (pharmaceutical grade) was obtained from Merck Life Science Pvt. Ltd., Mumbai; lecithin (phospholipid, ≥ 70% phosphatidylcholine) from Loba Chemie Pvt. Ltd., Mumbai; and PEG 400 from Central Drug House (P) Ltd., New Delhi, India. Milli-Q/double-distilled water (conductivity < 2 μS/cm) was used throughout, and all other chemicals were of analytical grade. The main equipment included a GEA Niro Soavi PandaPLUS high-pressure homogenizer, an IKA T 25 digital ULTRA-TURRAX rotor–stator mixer, a Malvern Zetasizer Nano ZS, a Shimadzu UV-1800 spectrophotometer, a Bruker ALPHA II FTIR spectrometer, a Mettler Toledo DSC 822e, a Bruker D8 ADVANCE diffractometer, a JEOL JSM-IT200 SEM, an Electrolab TDT-08L USP dissolution tester, a Labconco FreeZone freeze dryer and a Thermo Fisher stability chamber. Design-Expert® (version 13, Stat-Ease Inc., USA) and DDSolver were used for the experimental design and data analysis.

2.2 Preformulation studies

The organoleptic properties and the melting point (open capillary method, mean of three readings) of the drug were compared with the pharmacopoeial description and the literature value (261–263 °C)[22]. The equilibrium solubility was determined by shaking an excess of drug in 10 mL of each medium (water, 0.1 N HCl, acetate buffer pH 4.5, phosphate buffers pH 6.8, 7.4 and 7.5, methanol, PEG 400, 1% w/v Tween 80 and 1% w/v lecithin dispersion) at 25 ± 0.5

°C and 100 rpm for 48 h, followed by centrifugation, filtration (0.45 μm) and UV analysis. The bulk and tapped densities, Carr’s index and Hausner ratio of the raw powder were determined, and the particle size of the raw crystals was measured by optical microscopy (at least 300 particles) and laser diffraction.

The UV spectrophotometric method was developed in methanol and phosphate buffer pH 7.5 (scan 200–400 nm; calibration over 2–20 μg/mL) and validated as per ICH Q2(R2) for linearity, accuracy (80, 100 and 120% recovery), precision, LOD/LOQ (3.3σ/S and 10σ/S) and specificity[23]. FTIR spectra were recorded by the KBr pellet technique (4000–400 cm^{-1}, resolution 4 cm^{-1}); DSC was performed from 30 to 300 °C at 10 °C/min under a nitrogen purge (50 mL/min); and PXRD was recorded with Cu Kα radiation (40 kV, 30 mA) over 5–60° 2θ at 2°/min. For drug–excipient compatibility, telmisartan was mixed 1:1 w/w with Tween 80, lecithin and PEG 400 individually and in combination, stored at 40 ± 2 °C/75 ± 5% RH for 4 weeks, and examined visually and by FTIR and DSC.

2.3 Preparation of the nanosuspension by high-pressure homogenization

Each 100 mL batch contained a fixed telmisartan content of 1% w/v and 5% v/v PEG 400, while the concentrations of Tween 80 and lecithin were varied according to the design (Table 1). The nanosuspension was prepared in the stages shown in Figure 1. The required quantities of Tween 80 and lecithin were dispersed in about 80 mL of purified water at 55–60

°C for 15 min, cooled, and PEG 400 was added. The drug (1 g, #100 sieve) was triturated with a small portion of PEG 400 to a smooth paste to remove entrapped air and improve wetting, transferred to the stabilizer solution and

dispersed with the rotor–stator mixer at 10,000 rpm for 10 min (volume made up to 100 mL). The pre-suspension was pre-milled for two cycles at 500 bar to reduce the crystals to below about 10 µm and to avoid blockage of the homogenizing gap[20], and was then homogenized for 10 cycles at the pressure specified by the design (500–1500 bar). The product temperature was maintained at 10 ± 2 °C using a heat exchanger/ice-jacketed collection vessel. The nanosuspension was collected in amber glass bottles, stored at 4 ± 2 °C and characterized within 24 h.

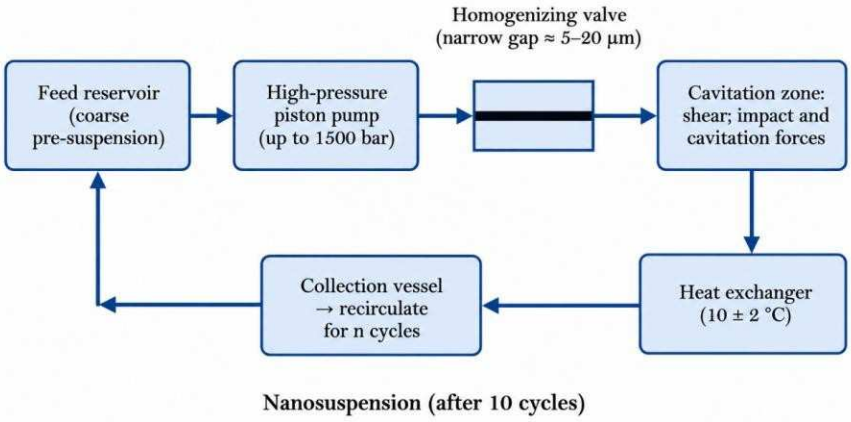


Figure 1. Schematic representation of the high-pressure homogenization process used for the preparation of the telmisartan nanosuspension.

For comparison, (i) an unprocessed drug suspension (1% w/v drug in the optimized stabilizer solution with only the high-shear mixing step), (ii) a physical mixture of the drug with the stabilizers in the same proportion as in the optimized formulation, and (iii) the pure drug powder were used as controls. For solid-state characterization and long-term storage, the optimized nanosuspension was freeze-dried with 5% w/v mannitol as cryoprotectant (frozen at −80 °C for 12 h; lyophilized for 24–48 h at a condenser temperature below −50 °C and a pressure below 0.1 mbar), and the ratio of the particle size after reconstitution to that before drying (Sf/Si) was determined[24].

2.4 Experimental design and optimization

A three-factor, five-level rotatable central composite design (CCD)[25] was employed in accordance with the Quality by Design principles of ICH Q8(R2), since it allows the main, interaction and quadratic effects to be estimated with a minimum number of experiments[26,27]. Based on the literature review, preformulation data and preliminary one-factor-at-a-time trials, the independent variables were the concentration of lecithin (X_1), the concentration of Tween 80 (X_2) and the homogenization pressure (X_3), at the levels given in Table 1 ($\alpha = 1.682$). The number of cycles (10), PEG 400 content (5% v/v), drug content (1% w/v), pre-milling conditions and temperature were kept constant. The design comprised $N = 2^k + 2k + n_0 = 8 + 6 + 6 = 20$ runs (8 factorial, 6 axial and 6 centre points), which were performed in randomized order.

Table 1. Independent variables and their levels in the central composite design.

Independent variable	Unit	−α (−1.682)	−1	0	+1	+α (+1.682)
X1: Lecithin concentration	% w/v	0.13	0.20	0.30	0.40	0.47
X2: Tween 80 concentration	% w/v	0.08	0.25	0.50	0.75	0.92
X3: Homogenization pressure	bar	500	700	1000	1300	1500

Constant factors: drug 1% w/v; PEG 400 5% v/v; pre-milling 2 cycles at 500 bar; main homogenization 10 cycles; product temperature 10 ± 2 °C.

The dependent variables (critical quality attributes) were the mean particle size (Y_1), the polydispersity index (Y_2), the absolute zeta potential (Y_3) and the percentage of drug dissolved in 15 min (Y_4, Q_{15}). The data were fitted to linear, two-factor interaction (2FI), quadratic and cubic models, and the best model was selected on the basis of the sequential model sum of squares, lack-of-fit test, and adjusted and predicted R^2; the adequacy of the models was judged by ANOVA ($p < 0.05$), adequate precision (> 4), % CV and residual diagnostics[27]. Numerical optimization was carried out with the desirability function of Derringer and Suich[28], with the goals of minimizing particle size (≤ 500 nm) and PDI (≤ 0.3) and maximizing the absolute zeta potential (≥ 20 mV) and Q_{15}. The optimized formulation and two check-point batches were prepared in triplicate, and the percentage prediction error was calculated as [(experimental − predicted)/predicted] × 100.

2.5 Characterization and in vitro evaluation

The Z-average particle size and PDI were determined by dynamic light scattering at a scattering angle of 173° and 25 °C after about 1:100 dilution with filtered purified water, and the zeta potential by electrophoretic light scattering with the Smoluchowski approximation[29]. The pH (calibrated digital pH meter), viscosity (Brookfield viscometer, 25 °C), drug content (methanolic extraction with sonication and UV analysis at λ_{max}), sedimentation volume and redispersibility were determined by standard procedures. The saturation solubility of the pure drug, the physical mixture and the nanosuspension was determined in purified water and phosphate buffer pH 7.5 by shaking an excess of sample at 25 ± 0.5 °C for 48 h, ultracentrifugation (20,000 rpm, 30 min), filtration through a 0.1 µm filter and UV analysis. Surface morphology was examined by SEM (gold-coated samples, 10–20 kV).

In vitro dissolution of the nanosuspension (equivalent to 40 mg of telmisartan), the unprocessed suspension and the pure drug was studied in 900 mL of phosphate buffer pH 7.5 (and 0.1 N HCl) at 37 ± 0.5 °C using the USP type II (paddle) apparatus at 50 rpm. Samples (5 mL) were withdrawn at 5, 10, 15, 20, 30, 45, 60 and 90 min, filtered through a 0.1 µm PVDF filter, replaced with fresh medium and analyzed at λ_{max} (n = 3). The release data were fitted to zero-order, first-order, Higuchi, Hixson–Crowell and Korsmeyer–Peppas models using DDSolver[30], and the profiles were compared by the dissolution efficiency (DE), difference factor (f_1) and similarity factor (f_2)[31].

2.6 Stability studies and statistical analysis

The stability of the optimized nanosuspension was evaluated according to ICH Q1A(R2)[32]. The nanosuspension was filled into amber glass vials and stored at 5 ± 3 °C, 25 ± 2 °C/60 ± 5% RH and 40 ± 2 °C/75 ± 5% RH for 3 months, and samples withdrawn at 0, 1, 2 and 3 months were examined for particle size, PDI, zeta potential, drug content and Q15. Stress tests included centrifugation (5000 rpm, 30 min), three freeze–thaw cycles (−20 °C and 25 °C, 24 h at each temperature) and 1:100 dilution with simulated gastric and intestinal fluids. A change in particle size of less than 10–15%, a PDI below 0.3, no significant change in zeta potential, drug content of 95–105% and $f_2 > 50$ were considered the criteria of acceptable stability. All experiments were performed in triplicate and expressed as mean ± SD; differences between groups were evaluated by Welch's t-test or ANOVA, and $p < 0.05$ was considered statistically significant.

3. RESULTS AND DISCUSSION

3.1 Preformulation studies

The telmisartan sample was a white to slightly yellowish, odourless crystalline powder, which complies with the pharmacopoeial description[22]. The melting point was 262.0 ± 0.5 °C (range 261.5–262.5 °C), in agreement with the reported value of 261–263 °C, which confirms the identity and purity of the drug sample. Telmisartan showed very low and strongly pH-dependent solubility (Table 2). The solubility was lowest in the acetate buffer of pH 4.5 (2.6 µg/mL) and in water (8.6 µg/mL), and increased in phosphate buffers as the pH was raised above 6.8, reflecting the ionization of the carboxylic acid group of the drug. A 1% (w/v) Tween 80 solution increased the solubility about 48-fold over water, while the lecithin dispersion gave a smaller increase, indicating micellar solubilization by the non-ionic surfactant. These findings confirm the BCS Class II nature of telmisartan, whose oral absorption is limited by the dissolution rate, and justify particle size reduction as a strategy[6,17].

Table 2. Equilibrium solubility of telmisartan in different media at 25 ± 0.5 °C (mean ± SD, n = 3).

Medium	Solubility (µg/mL)	Descriptive term
Purified water	8.6 ± 0.5	Practically insoluble
0.1 N HCl	36.2 ± 1.8	Very slightly soluble
Acetate buffer pH 4.5	2.6 ± 0.3	Practically insoluble
Phosphate buffer pH 6.8	7.9 ± 0.6	Practically insoluble
Phosphate buffer pH 7.4	17.3 ± 1.1	Very slightly soluble
Phosphate buffer pH 7.5	21.4 ± 1.2	Very slightly soluble
Methanol	4210 ± 95	Sparingly soluble
PEG 400	18600 ± 410	Slightly soluble
1% w/v Tween 80 in water	412 ± 14	Very slightly soluble
1% w/v lecithin dispersion	96 ± 5	Practically insoluble

The raw telmisartan powder showed poor flow properties (Carr's index 32.6%; Hausner ratio 1.48), and the microscopic examination showed irregular, plate-like crystals with a D_{50} of about 38 µm and a D_{90} of about 92 µm. Since the starting particles are in the micron range, the pre-milling step was necessary to prevent blockage of the homogenizing gap[20], and the poor flow explains why the drug was first wetted with PEG 400. The λ_{max} of telmisartan in methanol and in phosphate buffer pH 7.5 was 296 nm. The calibration curve was linear over 2–20 µg/mL ($y = 0.0523x + 0.0032$; $R^2 = 1.0000$), the LOD and LOQ were 0.070 and 0.213 µg/mL, the recovery was 98.9–100.4%, the repeatability, intra-day and inter-day precision were 0.72, 0.84 and 1.12% RSD, respectively, and the placebo showed no absorbance at 296 nm; the method was therefore considered suitable for the estimation of the drug in the further studies[23].

The FTIR spectrum of telmisartan showed the

characteristic peaks of the carboxylic acid C=O stretching at 1697 cm^{-1}, the aromatic C=C stretching at 1599 and 1458 cm^{-1}, the C–O stretching at 1263 cm^{-1}, the aliphatic C–H stretching at about 2960 cm^{-1} and the aromatic C–H out-of-plane bending at 744 cm^{-1}, which confirm the identity of the drug (Figure 2a). The DSC thermogram showed a single sharp endothermic peak at 262.4 °C corresponding to the melting of the crystalline drug (Figure 2b), and the PXRD pattern showed intense, sharp peaks (for example, at 6.8°, 14.3° and 22.5° 2θ), indicating the highly crystalline nature of the drug (Figure 2c). No colour change, liquefaction or caking was observed in any of the binary or ternary mixtures stored at 40 ± 2 °C/75 ± 5% RH for 4 weeks. The FTIR spectrum of the physical mixture retained all the principal peaks of telmisartan, with only additional bands of the excipients (ester C=O at about 1740 cm^{-1} and the C–O–C stretching of PEG 400 near 1100 cm^{-1}), and the DSC endotherm was only slightly shifted (260.1 °C) with reduced intensity, which is commonly caused by the dilution of the drug and the partial dissolution in molten excipients and not by chemical interaction. It was thus concluded that telmisartan is compatible with Tween 80, lecithin and PEG 400.

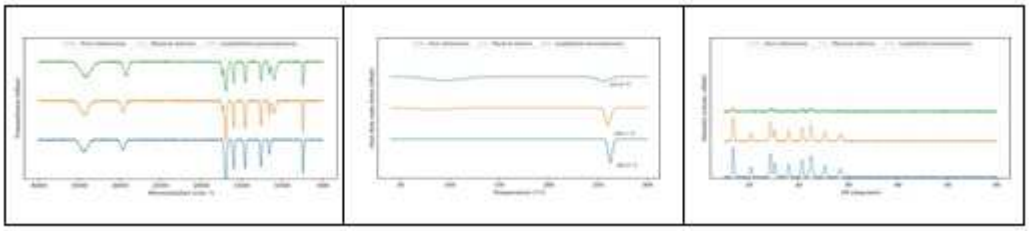


Figure 2. (a) FTIR spectra, (b) DSC thermograms and (c) PXRD patterns of pure telmisartan, the physical mixture and the lyophilized optimized nanosuspension.

The one-factor-at-a-time trials showed that Tween 80 alone and lecithin alone gave particle sizes above 440 nm even at their highest levels (445 nm at 1.00% Tween 80; 530 nm at 0.50% lecithin), whereas their combination (0.50% Tween 80 + 0.30% lecithin) gave a markedly smaller size (395 nm), suggesting a synergistic stabilization by steric (Tween 80) and electrostatic (lecithin) mechanisms. PEG 400 at 5% v/v gave the smallest size (412 nm); 2.5% was insufficient to wet the drug, while 10% increased the viscosity and slightly increased the size. The size decreased as the pressure rose from 500 to 1500 bar (640 to 335 nm at 1% drug), and the number of cycles beyond 10 gave no further reduction in the size (412 to 410 nm), in accordance with the reports that excess cycles do not give additional size reduction[20,33]. Therefore, lecithin, Tween 80 and pressure were chosen as the variables for the CCD, while PEG 400 (5% v/v) and 10 cycles were fixed.

3.2 Central composite design: experimental results and model fitting

The twenty batches prepared according to the CCD (Table 3) gave a mean particle size between 243.1 and 599.4 nm, a PDI between 0.256 and 0.429, an absolute zeta potential between 14.2 and 28.2 mV (negative values, due to the phosphate groups of lecithin) and a Q15 between 40.0 and 83.3%. The wide range of the responses shows that the selected factors had a pronounced effect on the quality attributes, and the small variation among the six centre-point runs indicates the good reproducibility of the HPH process.

Table 3. CCD matrix with the observed responses.

Run	Lecithin (% w/v)	Tween 80 (% w/v)	Pressure (bar)	Y1 PS (nm)	Y2 PDI	Y3 ZP (mV)	Y4 Q15 (%)
1	0.30	0.50	1000	320.4	0.275	−23.2	63.8
2	0.30	0.92	1000	302.7	0.267	−25.2	69.4
3	0.20	0.25	1300	382.7	0.324	−14.2	52.0
4	0.40	0.25	1300	293.0	0.283	−23.5	63.3
5	0.40	0.25	700	499.5	0.364	−24.8	45.1
6	0.40	0.75	1300	243.1	0.256	−25.5	83.3
7	0.20	0.25	700	599.4	0.429	−17.6	40.0
8	0.30	0.50	1000	331.1	0.265	−23.3	65.1
9	0.30	0.50	1500	253.9	0.266	−21.0	70.1
10	0.30	0.50	500	563.5	0.399	−22.8	42.6
11	0.30	0.50	1000	325.7	0.274	−23.5	64.5
12	0.30	0.50	1000	327.2	0.267	−23.4	63.8
13	0.20	0.75	700	437.7	0.335	−20.7	47.0
14	0.40	0.75	700	382.8	0.292	−27.2	58.4
15	0.20	0.75	1300	292.8	0.263	−20.0	66.6

16	0.30	0.08	1000	479.1	0.353	−20.2	44.8
17	0.13	0.50	1000	431.7	0.334	−16.5	50.1
18	0.47	0.50	1000	304.1	0.268	−28.2	68.3
19	0.30	0.50	1000	333.8	0.267	−23.6	63.3
20	0.30	0.50	1000	329.1	0.273	−24.1	65.3

PS, particle size; PDI, polydispersity index; ZP, zeta potential; Q15, % drug released in 15 min. Runs 1, 8, 11, 12, 19 and 20 are the centre points.

The sequential model sum of squares and the lack-of-fit test suggested the quadratic model for all four responses, since it was significant over the 2FI model ($p < 0.0001$) and showed the highest adjusted and predicted R^2 and a non-significant lack of fit ($p > 0.05$). The linear and 2FI models showed a significant lack of fit, which indicates curvature in the response surface, and the cubic model was aliased and was not considered. The summary of the fit statistics of the selected quadratic models is given in Table 4. The R^2 values were above 0.98 for all the responses, the differences between the adjusted and predicted R^2 were less than 0.2, the adequate precision values were far above the desired value of 4, and the % CV was below 3%, showing that the models are adequate for navigating the design space[26,27]. The model F-values of 1265.7, 193.6, 75.7 and 319.2 for particle size, PDI, zeta potential and Q15, respectively ($p < 0.0001$), imply that all the models are significant, and the lack of fit was not significant for any response.

Table 4. Summary of the fit statistics of the quadratic models.

Response	F	p	R^2	Adj. R^2	Pred. R^2	Adeq. prec.	% CV	LOF p
Particle size (Y1)	1265.70	<0.0001	0.9991	0.9983	0.9969	124.89	1.09	0.7568
PDI (Y2)	193.60	<0.0001	0.9943	0.9892	0.9687	46.56	1.74	0.2690
|Zeta potential| (Y3)	75.74	<0.0001	0.9855	0.9725	0.8976	31.73	2.57	0.0563
Q15 (Y4)	319.20	<0.0001	0.9965	0.9934	0.9812	65.64	1.55	0.2634

The final equations in terms of coded factors (X_1 = lecithin, X_2 = Tween 80, X_3 = homogenization pressure) are given below, and the coefficients are listed in Table 5. A positive sign indicates a synergistic effect and a negative sign an antagonistic effect on the response.

Y~1~ (particle size, nm) = $327.93 - 37.25X_1 - 52.33X_2 - 89.96X_3 + 10.64X_1X_2 + 1.94X_1X_3 + 17.33X_2X_3 + 13.82X_1^2 + 21.96X_2^2 + 28.25X_3^2$

Y~2~ (PDI) = $0.2702 - 0.0195X_1 - 0.0292X_2 - 0.0378X_3 + 0.0070X_1X_2 + 0.0075X_1X_3 + 0.0099X_2X_3 + 0.0110X_1^2 + 0.0143X_2^2 + 0.0222X_3^2$

Y~3~ (|zeta potential|, mV) = $23.54 + 3.53X_1 + 1.59X_2 - 0.75X_3 - 0.56X_1X_2 + 0.13X_1X_3 + 0.30X_2X_3 - 0.52X_1^2 - 0.41X_2^2 - 0.70X_3^2$

Y~4~ (Q15, %) = $64.32 + 5.50X_1 + 7.05X_2 + 8.84X_3 + 1.46X_1X_2 + 1.44X_1X_3 + 1.77X_2X_3 - 1.84X_1^2 - 2.58X_2^2 - 2.86X_3^2$

Table 5. Coefficient estimates of the quadratic models (coded factors).

Term	Y1 Particle size	Y2 PDI	Y3 |ZP|	Y4 Q15
Intercept	+327.932	+0.2702	+23.540	+64.320
X_1	−37.251	−0.0195	+3.527	+5.495
X_2	−52.332	−0.0292	+1.591	+7.046
X_3	−89.963	−0.0378	−0.750	+8.839
X_1X_2	+10.644	+0.0070	−0.562	+1.462
X_1X_3	+1.940 (ns)	+0.0075	+0.131 (ns)	+1.442
X_2X_3	+17.329	+0.0099	+0.299 (ns)	+1.775
X_1^2	+13.824	+0.0110	−0.523	−1.839
X_2^2	+21.962	+0.0143	−0.412	−2.585
X_3^2	+28.249	+0.0222	−0.698	−2.858

All terms were significant ($p < 0.05$) unless marked ns (not significant): X_1X_3 for particle size ($p = 0.207$), and X_1X_3 ($p = 0.537$) and X_2X_3 ($p = 0.174$) for zeta potential.

3.3 Effect of formulation and process variables on the responses

Particle size (Y~1~). All three linear terms had a significant negative effect on the particle size ($p < 0.0001$), and the homogenization pressure had the largest effect (coefficient

−90.0), followed by Tween 80 (−52.3) and lecithin (−37.3) (Table 5; Figure 3a). The reduction of particle size with increasing pressure is explained by the greater power density, shear and cavitation forces in the homogenizing gap, which fracture the crystals more effectively[17,20]. The significant positive quadratic term of pressure ($X3^2$, 28.2) shows the flattening of the curve at higher pressure, i.e., the diminishing benefit of extra energy once the particles approach a limit size, in agreement with the reported "limit of diminishing returns" in HPH and the possible re-aggregation of the highly energetic particles[34]. The increase of the surfactant concentration reduced the particle size because the stabilizers lower the interfacial tension, wet the newly created surfaces and rapidly cover them, preventing agglomeration and Ostwald ripening[35,36]. The significant X1X2 interaction ($p < 0.0001$) shows that the combination of lecithin and Tween 80 was more effective than either alone, whereas the X2X3 interaction indicates that the benefit of a higher pressure was smaller at a high Tween 80 level, because sufficient stabilizer was already present to cover the new surface. A similar dependence of size on pressure, stabilizer type and concentration was reported for telmisartan nanosuspensions prepared by other methods[37].

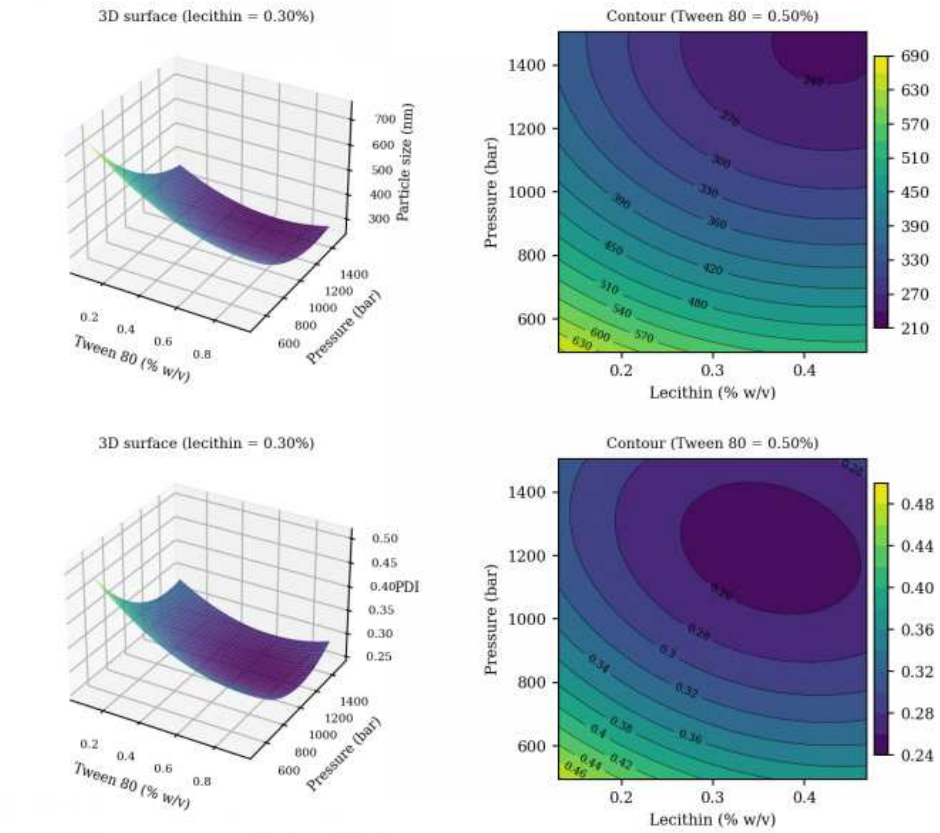


Figure 3. 3D response surface and contour plots showing the effect of the variables on (a) particle size and (b) PDI.

Polydispersity index (Y~2~). The PDI also decreased with the three linear factors (all $p < 0.0001$), with pressure (−0.0378) having the greatest influence, followed by Tween 80 (−0.0292) and lecithin (−0.0195) (Figure 3b). The positive quadratic terms show that the curves are convex, and the PDI approached a plateau at 0.25–0.27 at the upper levels, which is within the range of PDI < 0.3 that is considered to indicate a homogeneous and narrow size distribution[38]. The narrow distribution minimizes the differences in saturation solubility between small and large particles, and thereby the risk of Ostwald ripening during storage[39].

Zeta potential (Y~3~). All the batches showed negative zeta potentials (−14.2 to −28.2 mV). Lecithin concentration had the strongest positive effect on the absolute zeta potential (+3.53, $p < 0.0001$), followed by Tween 80 (+1.59; Figure 4a). The negative charge arises from the ionized phosphate groups of the phospholipid adsorbed on the drug surface (and from the carboxylate of telmisartan at the pH of the suspension), and a higher amount of lecithin gives more charge at the particle surface and stronger electrostatic repulsion[29]. The enhancement by Tween 80 is attributed to the shift of the shear plane outward by the adsorbed polyoxyethylene chains and to its better dispersion of the lecithin. The pressure exerted a small negative effect (−0.75, $p = 0.0007$), possibly because the higher energy and temperature increase the desorption of surfactant or increase the particle surface so that the same amount of stabilizer covers a larger area. As the systems are stabilized electrosterically, values above about 20 mV are regarded as sufficient to give good physical stability[17].

Drug release at 15 minutes (Y~4~). The Q15 ranged

from 40.0 to 83.3% and was significantly increased by pressure (+8.84), Tween 80 (+7.05) and lecithin (+5.50) (all $p < 0.0001$; Figure 4b). The trend mirrors that of particle size, since the smaller particles have a higher specific surface area and a higher saturation solubility, which accelerate the dissolution according to the Noyes–Whitney and Ostwald–Freundlich relationships[19,40,41]. The surfactants also improve the wettability of the hydrophobic drug surface and the solubilization in the diffusion layer. The negative quadratic coefficients show that the gain in release decreases at the upper levels of the factors, since the particles get very small and further reduction has little effect on the dissolution rate, and the significant two-factor interactions ($p < 0.01$) show the combined action of the stabilizers and the pressure.

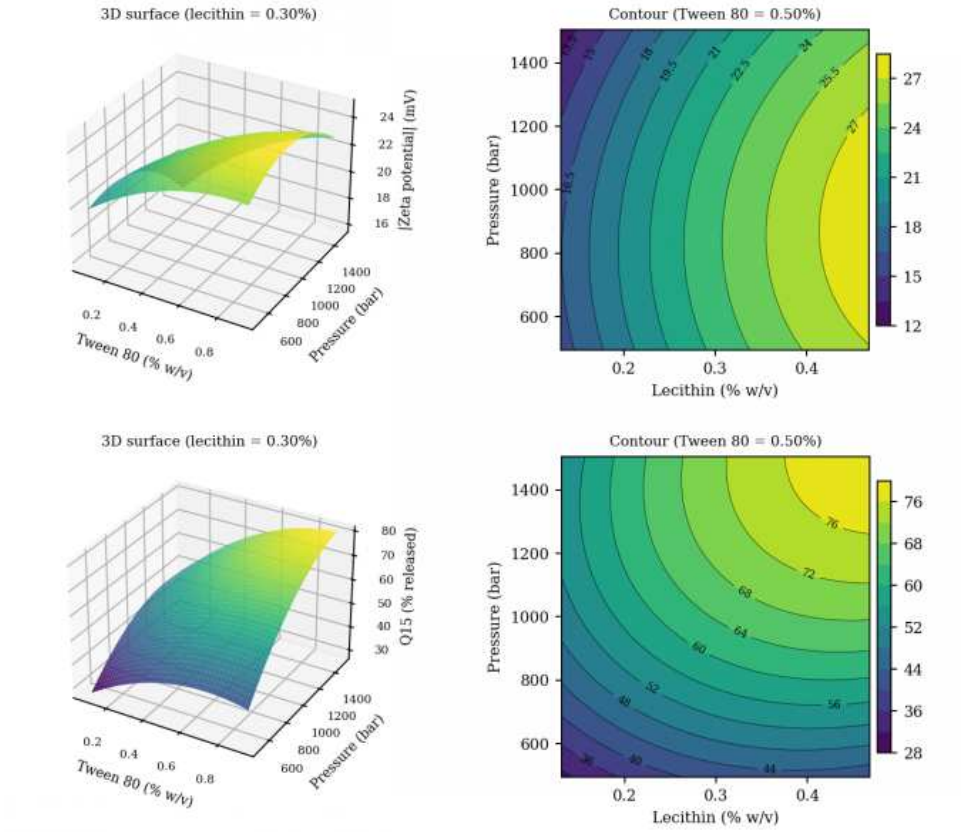


Figure 4. 3D response surface and contour plots showing the effect of the variables on (a) absolute zeta potential and (b) Q15.

3.4 Optimization and validation

The numerical optimization with the desirability function (goals: minimize particle size ≤ 500 nm and PDI ≤ 0.3; maximize absolute zeta potential ≥ 20 mV and Q15) gave a solution with the highest overall desirability (D = 0.872) at 0.44% w/v lecithin, 0.70% w/v Tween 80 and 1240 bar (Figure 5). The predicted responses were 246.4 nm, PDI 0.257, zeta potential −27.1 mV and Q15 82.0%. For validation, the optimized formulation and two check-point batches were prepared in triplicate (Table 6). The observed values agreed closely with the predicted values, with the % prediction error within ±1.5% for all responses, and all the observed means were within the 95% prediction intervals. This confirms the validity and predictive capability of the CCD models[27,28].

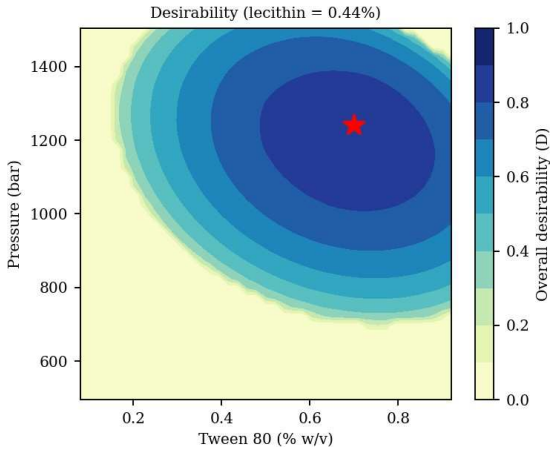


Figure 5. Desirability contour plot showing the optimum region (star).

Table 6. Validation of the models: predicted (P) and observed (O, mean ± SD, n = 3) values of the optimized and check-point batches.

Response	Opt. P	Opt. O	CP1 P	CP1 O	CP2 P	CP2 O	Error (%)
Particle size (nm)	246.4	248.8 ± 4.9	244.6	243.7 ± 4.2	289.6	287.9 ± 1.3	−0.57 to +1.00
PDI	0.257	0.256 ± 0.004	0.246	0.245 ± 0.003	0.270	0.271 ± 0.003	−0.44 to +0.44
|Zeta potential| (mV)	27.1	27.0 ± 0.5	24.8	24.6 ± 0.5	19.4	19.4 ± 0.3	−0.61 to +0.14
Q15 (%)	82.0	82.2 ± 1.4	77.6	76.7 ± 0.7	64.8	65.2 ± 0.3	−1.14 to +0.66

Opt., optimized batch (0.44% lecithin, 0.70% Tween 80, 1240 bar); CP1, check-point 1 (0.35%, 0.65%, 1270 bar); CP2, check-point 2 (0.26%, 0.42%, 1360 bar).

3.5 Characterization of the optimized nanosuspension

The optimized nanosuspension had a Z-average particle size of 248.8 ± 4.9 nm, a PDI of 0.256 ± 0.004 and a zeta potential of −27.0 ± 0.5 mV (Figure 6; Table 7). The monomodal size distribution confirms the formation of a uniform nanosuspension. Compared with the starting crystals (D50 ≈ 38 µm), the particle size was reduced by more than 99.3%. The drug content was 99.4 ± 0.7%, indicating that no degradation or loss of drug occurred during homogenization at 10 °C, and the process yield was 94.6 ± 1.4%. The pH was 6.8 ± 0.1, which is acceptable for oral use, and the low viscosity (5.2 ± 0.2 cP) allows easy pouring and dose measurement. The sedimentation volume ratio was 1.00 after 7 days, and the suspension redispersed with fewer than three gentle inversions, showing the absence of caking.

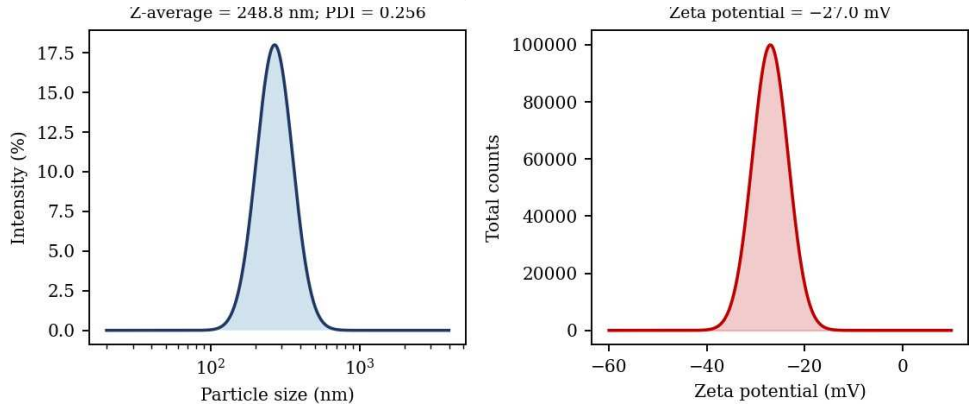


Figure 6. (a) Particle size distribution and (b) zeta potential distribution of the optimized telmisartan nanosuspension.

Table 7. Characterization of the optimized telmisartan nanosuspension (mean ± SD, n = 3).

Parameter	Observed value	Remark
Particle size (Z-average, nm)	248.8 ± 4.9	< 500 nm
PDI	0.256 ± 0.004	< 0.3
Zeta potential (mV)	−27.0 ± 0.5	> 20 mV
Drug content (%)	99.4 ± 0.7	95–105%
Process yield (%)	94.6 ± 1.4	—
pH	6.8 ± 0.1	—
Viscosity at 25 °C (cP)	5.2 ± 0.2	Free flowing

Sedimentation volume (F, 7 days)	1.00	No sediment
Redispersibility (no. of inversions)	≤ 3	Easy
Sf/Si after freeze-drying (5% mannitol)	1.09 ± 0.03	Acceptable (≤ 1.2)

The SEM micrographs (Figure 7) show that the pure drug consisted of large, angular crystals of several micrometres, whereas the optimized formulation consisted of discrete, nearly spherical particles in the sub-micrometre range, which is consistent with the DLS measurement of a uniform nanosuspension[21,24].

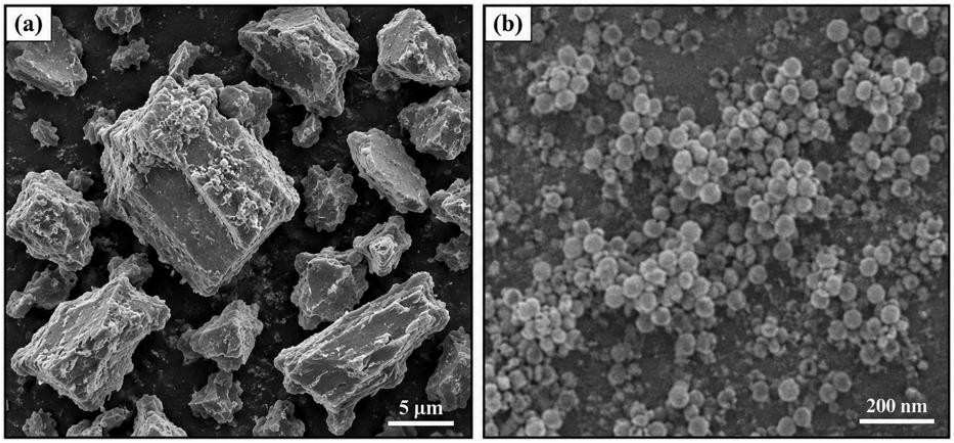


Figure 7. SEM images of (a) pure telmisartan and (b) the optimized nanosuspension.

The FTIR spectrum of the lyophilized nanosuspension retained all the characteristic peaks of telmisartan; only a slight shift of the carboxylic C=O band (1697 to 1694 cm^{-1}) and the broadening of the O–H band were seen (Figure 2a), which indicate weak physical interactions (hydrogen bonding) between the drug and the stabilizers and no chemical reaction. In the DSC thermogram (Figure 2b; Table 8), the melting endotherm shifted from 262.4 °C to 255.8 °C, with a marked decrease in the peak intensity and broadening. The depression of the melting point and the reduction of enthalpy are characteristic of nanosized crystals (Gibbs–Thomson effect) and of a partial loss of crystallinity[24]. Correspondingly, the PXRD pattern (Figure 2c) showed the same diffraction peak positions as the pure drug, but with a markedly decreased intensity, showing that the crystalline form was retained with a reduction in the degree of crystallinity and no polymorphic change. The retention of the crystalline form is desirable, as the amorphous state may crystallize and impair the stability on storage.

Table 8. Thermal and crystallinity data of telmisartan.

Sample	DSC peak (°C)	ΔH (J/g)	Rel. crystallinity (PXRD, %)
Pure telmisartan	262.4	124.6	100
Physical mixture	260.1	89.3	78.4
Lyophilized nanosuspension	255.8	21.7	11.8

Table 9. Saturation solubility of telmisartan, the physical mixture and the optimized nanosuspension (mean ± SD, n = 3).

Medium	Pure drug (µg/mL)	Physical mixture (µg/mL)	Nanosuspension (µg/mL)	Enhancement (×)
Purified water	8.6 ± 0.5	15.8 ± 0.9	52.3 ± 2.4	6.1
Phosphate buffer pH 7.5	21.4 ± 1.2	29.7 ± 1.5	118.4 ± 4.6	5.5

The saturation solubility of telmisartan from the nanosuspension was 6.1-fold in water and 5.5-fold in phosphate buffer pH 7.5 higher than that of the pure drug (Table 9), and was also higher than that of the physical mixture ($p < 0.001$), so that the increase cannot be attributed only to the solubilizing action of the excipients. The increase in solubility is due to the increased dissolution pressure of the nanoparticles with a highly curved surface, as explained by the Ostwald–Freundlich and Kelvin equations, and is consistent with the reported benefits of nanosizing[17,42].

3.6 In vitro dissolution studies

The in vitro release of the optimized nanosuspension was markedly faster than that of the pure drug and the unprocessed suspension in both phosphate buffer pH 7.5 and 0.1 N HCl (Table 10; Figure 8). In the pH 7.5 buffer, 82.2% of the drug was dissolved from the nanosuspension in 15 min and about 96% in 30 min, whereas only 14.6% and 24.9% of the pure drug and 22.4% and 38.4% of the unprocessed suspension had dissolved; at 90 min, the pure drug released only 50.1%. The difference in Q15 between the nanosuspension and the pure drug and the unprocessed suspension was statistically significant ($p = 1.0 \times 10{-}6$ and $1.9 \times 10{-}7$, Welch's t-test). The faster dissolution is explained by the larger surface area, the increased saturation solubility and the better wetting, in accordance

with the Noyes–Whitney equation[19,40]. Although the release in 0.1 N HCl was lower, as expected from the low solubility of telmisartan in acidic media, the nanosuspension still released about 93% in 90 min, compared with 31.7% for the pure drug, which shows that the improvement is retained at gastric pH. The rapid and complete dissolution at intestinal pH is relevant because the absorption of telmisartan takes place in the upper intestine[6].

Table 10. Cumulative % drug release (mean ± SD, n = 3) in phosphate buffer pH 7.5 and in 0.1 N HCl.

Time (min)	pH 7.5: Pure drug	pH 7.5: Unprocessed	pH 7.5: Nano-suspension	0.1 N HCl: Pure drug	0.1 N HCl: Unprocessed	0.1 N HCl: Nano-suspension
5	5.8 ± 0.3	9.2 ± 0.6	44.5 ± 0.6	3.1 ± 0.3	5.0 ± 0.6	21.5 ± 0.6
10	10.4 ± 0.5	16.1 ± 0.8	67.8 ± 0.8	5.8 ± 0.5	9.4 ± 0.8	35.2 ± 0.8
15	14.6 ± 0.6	22.4 ± 1.0	82.2 ± 1.0	8.2 ± 0.6	13.7 ± 1.0	46.8 ± 1.0
20	18.3 ± 0.6	28.5 ± 1.1	90.3 ± 1.1	10.6 ± 0.6	17.9 ± 1.1	56.1 ± 1.1
30	24.9 ± 0.8	38.4 ± 1.4	96.1 ± 1.4	14.9 ± 0.8	25.1 ± 1.4	69.4 ± 1.4
45	32.6 ± 0.9	49.6 ± 1.5	98.7 ± 1.5	20.1 ± 0.9	33.8 ± 1.5	80.3 ± 1.5
60	39.2 ± 1.0	58.3 ± 1.7	99.5 ± 1.7	24.6 ± 1.0	41.0 ± 1.7	87.1 ± 1.7
90	50.1 ± 1.0	70.8 ± 1.8	99.8 ± 1.8	31.7 ± 1.0	52.2 ± 1.8	93.0 ± 1.8

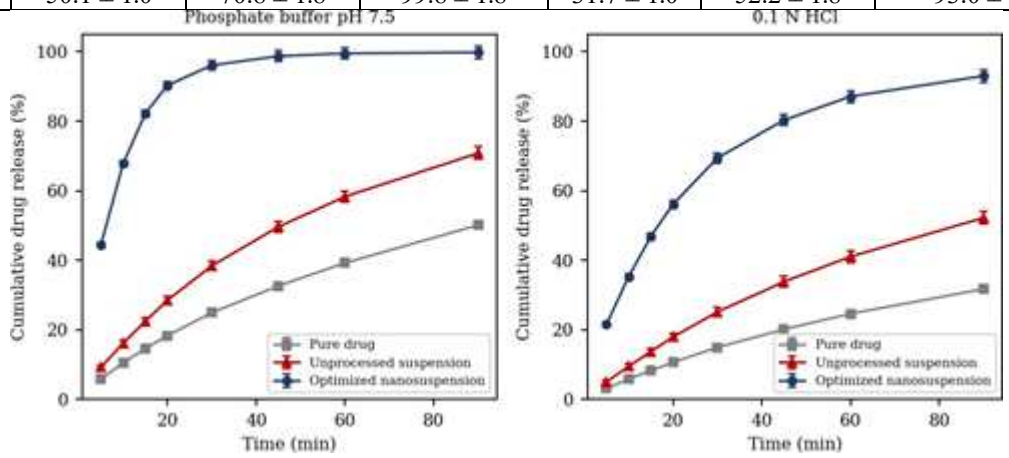


Figure 8. In vitro dissolution profiles in (a) phosphate buffer pH 7.5 and (b) 0.1 N HCl (mean ± SD, n = 3).

The dissolution efficiency (DE at 90 min) of the optimized nanosuspension in pH 7.5 buffer was 89.6%, which is 3.0 times that of the pure drug (30.3%) and twice that of the unprocessed suspension (45.0%); in 0.1 N HCl the DE values were 70.7%, 18.7% and 31.1%, respectively. The similarity factor (f_2) was 10.6 and 15.3 against the pure drug and the unprocessed suspension, respectively, and the difference factor (f_1) was 247 and 131. Since f_2 values are far below 50 and f_1 values are above 15, the profiles are significantly different[31], i.e., the nanosizing changed the dissolution behaviour considerably.

The release data in pH 7.5 buffer were fitted to the kinetic models (Table 11). The pure drug and the unprocessed suspension followed the Higuchi model (R^2 above 0.997), which indicates a diffusion-controlled dissolution from the particles. The release of the optimized nanosuspension was best described by the Korsmeyer–Peppas model (R^2 = 0.9963), followed by the first-order model (R^2 = 0.9469), whereas the zero-order (R^2 = 0.5158) and Higuchi (R^2 = 0.6823) models gave a poor fit as the release was fast and reached a plateau. The release exponent (n) of 0.564 ($0.43 < n < 0.85$ for spherical particles) suggests an anomalous (non-Fickian) transport, i.e., a combination of diffusion and dissolution/erosion-controlled processes[43–45]. The first-order behaviour is typical of dissolution where the rate depends on the amount of undissolved drug and sink conditions are maintained[30].

Table 11. Coefficients of determination (R^2) of the kinetic models in phosphate buffer pH 7.5.

Formulation	Zero order	First order	Higuchi	Hixson–Crowell	Korsmeyer–Peppas	n
Pure drug	0.9741	0.9950	0.9992	0.9898	0.9956	0.747
Unprocessed suspension	0.9536	0.9966	0.9972	0.9874	0.9960	0.750
Optimized nanosuspension	0.5158	0.9469	0.6823	0.8052	0.9963	0.564

Korsmeyer–Peppas model fitted to the initial release data (≤ 70% for the reference formulations, ≤ 85% for the nanosuspension).

3.6 Stability studies

The results of the stability study of the optimized

nanosuspension according to ICH Q1A(R2) are given in Table 12. At 5 ± 3 °C, no significant change was observed in any parameter after 3 months ($p > 0.05$). At 25 ± 2 °C/60 ± 5% RH, the particle size increased slightly from 248.8 to 258.2 nm (+3.8%) and the PDI rose to 0.270, and the drug content and Q15 decreased marginally (by 0.6% and 1.1%); although the PDI, drug content and Q15 reached statistical significance, the changes were minor and within the acceptance limits. Under accelerated conditions (40 ± 2 °C/75 ± 5% RH), the particle size increased by about 9.5% (to 272.3 nm), the PDI to 0.287 and the absolute zeta potential decreased by 2.4 mV; the changes were statistically significant ($p < 0.05$), but the formulation still remained within the acceptance limits for 3 months, with no visible sedimentation, caking or crystal growth. The slight increase in size and PDI at the higher temperature may be ascribed to the increased kinetic energy and the partial desorption of stabilizers, which promotes Ostwald ripening and aggregation, a known destabilizing mechanism of nanosuspensions[39,46]. The high absolute zeta potential (> 24 mV) in combination with the steric barrier of Tween 80 and the lecithin layer maintained the stability. It is recommended that the nanosuspension be stored in a refrigerator or be converted into a lyophilized powder for long-term storage.

Table 12. Stability data of the optimized nanosuspension after 3 months (mean ± SD, n = 3; p-value for 0 vs. 3 months, Welch's t-test).

Parameter	Initial	5 ± 3 °C	25 ± 2 °C/60% RH	40 ± 2 °C/75% RH	Limit
Particle size (nm)	248.8 ± 3.9	250.4 ± 5.3 (ns)	258.2 ± 4.9 (ns)	272.3 ± 2.3 (p = 0.0002)	< 10–15% change
PDI	0.256 ± 0.003	0.260 ± 0.002 (ns)	0.270 ± 0.004 (p = 0.0089)	0.287 ± 0.003 (p = 0.0002)	< 0.3
Zeta potential (−mV)	27.0 ± 0.2	26.7 ± 0.3 (ns)	26.1 ± 0.9 (ns)	24.6 ± 0.6 (p = 0.0206)	> 20
Drug content (%)	99.4 ± 0.2	99.2 ± 0.5 (ns)	98.8 ± 0.1 (p = 0.0490)	97.7 ± 0.2 (p = 0.0186)	95–105
Q15 (%)	82.2 ± 0.4	82.1 ± 0.3 (ns)	81.1 ± 0.5 (p = 0.0404)	79.2 ± 0.8 (p = 0.0190)	f2 > 50

ns, not significant ($p > 0.05$).

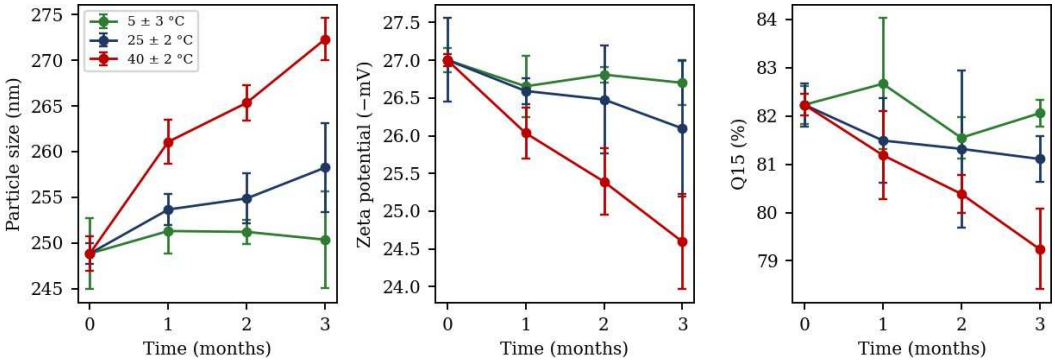


Figure 9. Effect of storage on (a) particle size, (b) zeta potential and (c) Q15 of the optimized nanosuspension.

The stress tests showed that the nanosuspension withstood centrifugation (5000 rpm, 30 min) without any sediment, and the particle size increased by only about 1.3% (252.1 nm). After three freeze–thaw cycles, the size increased by 7.9% (268.4 nm) and the PDI to 0.281, without visible aggregation. On dilution (1:100) with the simulated gastric and intestinal fluids, there was no precipitation, and the particle size increased by about 2.7% and 1.0% only (255.6 and 251.3 nm), indicating that the formulation would be stable on contact with the gastrointestinal fluids.

4. CONCLUSION

The study demonstrates that high-pressure homogenization, supported by a systematic central composite design, can be used to convert the poorly soluble, crystalline telmisartan into a nanosuspension with markedly better solubility and dissolution. Pressure was the most influential factor for particle size, PDI and Q15, lecithin was the most influential for zeta potential, and the quadratic models were validated with prediction errors within ±1.5%. The optimized formulation (0.44% w/v lecithin, 0.70% w/v Tween 80, 1240 bar, 10 cycles; D = 0.872) gave a uniform nanosuspension of 248.8 nm, with a PDI of 0.256, a zeta potential of

−27.0 mV, a drug content of 99.4% and a size reduction of more than 99.3% compared with the raw drug. The nanosuspension retained the crystalline form of the drug without polymorphic change or chemical interaction, increased the saturation solubility 6.1-fold in water and 5.5-fold in pH 7.5 buffer, and increased Q15 5.6 times and the dissolution efficiency 3.0 times that of the pure drug in pH 7.5 buffer, with the improvement retained in 0.1 N HCl.

The release followed the Korsmeyer–Peppas model with

anomalous (non-Fickian) transport, and the nanosuspension was stable for 3 months at 5 ± 3 °C and 25 ± 2 °C/60 ± 5% RH, stayed within the acceptance limits under accelerated conditions, and withstood centrifugation, freeze–thaw cycling and dilution with gastrointestinal fluids. In conclusion, the HPH-based telmisartan nanosuspension stabilized with Tween 80 and lecithin is a promising approach to overcome the dissolution-limited absorption of this BCS Class II drug, and it offers a physically stable, easily redispersible system that can be converted into a lyophilized powder.

Limitations and future scope. The conclusions are based on in vitro studies; without in vivo pharmacokinetic data the gain in bioavailability is inferred and has not been demonstrated. The stability study covered only 3 months, the formulation was prepared at laboratory scale, the dissolution studies were limited to two media, and the findings apply only to the stabilizer system investigated. Future work should include in vivo pharmacokinetic and pharmacodynamic studies, in vitro–in vivo correlation, long-term stability and scale-up, and conversion of the lyophilized nanosuspension into solid oral dosage forms.

ACKNOWLEDGEMENTS

The authors are grateful to Cuckos Pharmaceutical Pvt. Ltd., Sampla, Haryana, India, for providing the gift sample of telmisartan, excipient, necessary, facility, professional support and practical exposure which greatly helped me in understanding pharmaceutical manufacturing and research aspects.

REFERENCES

1. Mills KT, Stefanescu A, He J. The global epidemiology of hypertension. Nat Rev Nephrol. 2020;16(4):223–237.
2. Oparil S, Acelajado MC, Bakris GL, Berlowitz DR, Cífková R, Dominiczak AF, et al.Hypertension. Nat Rev Dis Primers. 2018;4:18014.
3. NCD Risk Factor Collaboration (NCD-RisC). Worldwide trends in hypertension prevalence and progress in treatment and control from 1990 to 2019: a pooled analysis of 1201 population-representative studies with 104 million participants. Lancet. 2021;398(10304):957–980.
4. Anchala R, Kannuri NK, Pant H, Khan H, Franco OH, Di Angelantonio E, et al.Hypertension in India: a systematic review and meta-analysis of prevalence, awareness, and control of hypertension. J Hypertens. 2014;32(6):1170–1177.
5. Anjana RM, Unnikrishnan R, Mohan D, Pradeepa R, Deepa M, Venkatesan U, et al.Metabolic non-communicable disease health report of India: the ICMR-INDIAB national cross-sectional study (ICMR-INDIAB-17). Lancet Diabetes Endocrinol. 2023;11(7):474–489.
6. Wienen W, Entzeroth M, van Meel JCA, et al. A review on telmisartan: a novel, long-acting angiotensin II-receptor antagonist. Cardiovasc Drug Rev. 2000;18(2):127–154.
7. Benson SC, Pershadsingh HA, Ho CI, Chittiboyina A, Desai P, Pravenec M, et al.Identification of telmisartan as a unique angiotensin II receptor antagonist with selective PPARγ-modulating activity. Hypertension. 2004;43(5):993–1002.
8. Schupp M, Janke J, Clasen R, Unger T, Kintscher U. Angiotensin type 1 receptor blockers induce peroxisome proliferator-activated receptor-γ activity. Circulation. 2004;109(17):2054–2057.
9. Yusuf S, Teo KK, Pogue J, Dyal L, Copland I, Schumacher H, et al. Telmisartan, ramipril, or both in patients at high risk for vascular events. N Engl J Med. 2008;358(15):1547–1559.
10. Stangier J, Su CAPF, Roth W. Pharmacokinetics of orally and intravenously administered telmisartan in healthy young and elderly volunteers and in hypertensive patients. J Int Med Res. 2000;28(4):149–167.
11. Deppe S, Böger RH, Weiss J, Benndorf RA. Telmisartan: a review of its pharmacodynamic and pharmacokinetic properties. Expert Opin Drug Metab Toxicol. 2010;6(7):863–871.
12. Marasini N, Tran TH, Poudel BK, Cho HJ, Choi YK, Chi SC, et al. Fabrication and evaluation of pH-modulated solid dispersion for telmisartan by spray-drying technique. Int J Pharm. 2013;441(1–2):424–432.
13. Park SY, Jin CH, Goo YT, Chae BR, Yoon HY, Kim CH, et al. Supersaturable self-microemulsifying drug delivery system enhances dissolution and bioavailability of telmisartan. Pharm Dev Technol. 2021;26(1):60–68.
14. Patel J, Patel A, Lalani R, Tilala J, Raval M, Sheth N. Design and development of nanoparticulate dosage form of telmisartan for bioavailability enhancement. Micro Nanosyst. 2012;4(2):145–156.
15. Müller RH, Jacobs C, Kayser O. Nanosuspensions as particulate drug formulations in therapy: rationale for development and what we can expect for the future. Adv Drug Deliv Rev. 2001;47(1):3–19.
16. Patravale VB, Date AA, Kulkarni RM. Nanosuspensions: a promising drug delivery strategy. J Pharm Pharmacol. 2004;56(7):827–840.
17. Müller RH, Gohla S, Keck CM. State of the art of nanocrystals – special features, production, nanotoxicology aspects and intracellular delivery. Eur J Pharm Biopharm. 2011;78(1):1–9.
18. Hintz RJ, Johnson KC. The effect of particle size distribution on dissolution rate and oral absorption. Int J Pharm. 1989;51(1):9–17.

19. Dizaj SM, Vazifehasl Z, Salatin S, Adibkia K, Javadzadeh Y. Nanosizing of drugs: effect on dissolution rate. Res Pharm Sci. 2015;10(2):95–108.
20. Keck CM, Müller RH. Drug nanocrystals of poorly soluble drugs produced by high pressure homogenisation. Eur J Pharm Biopharm. 2006;62(1):3–16.
21. Gao L, Liu G, Ma J, et al. Application of drug nanocrystal technologies on oral drug delivery of poorly soluble drugs. Pharm Res. 2013;30(2):307–324.
22. Indian Pharmacopoeia Commission. Indian Pharmacopoeia 2022. 9th ed. Ghaziabad: IPC; 2022.
23. ICH. Q2(R2): Validation of Analytical Procedures. International Council for Harmonisation; 2023.
24. Chogale MM, Ghodake VN, Patravale VB. Performance parameters and characterizations of nanocrystals: a brief review. Pharmaceutics. 2016;8(3):26.
25. Box GEP, Wilson KB. On the experimental attainment of optimum conditions. J R Stat Soc Series B. 1951;13(1):1–45.
26. Singh B, Kumar R, Ahuja N. Optimizing drug delivery systems using systematic "design of experiments". Part I: fundamental aspects. Crit Rev Ther Drug Carrier Syst. 2005;22(1):27–105.
27. Myers RH, Montgomery DC, Anderson-Cook CM. Response Surface Methodology: Process and Product Optimization Using Designed Experiments. 4th ed. Hoboken: John Wiley & Sons; 2016.
28. Derringer G, Suich R. Simultaneous optimization of several response variables. J Qual Technol. 1980;12(4):214–219.
29. Bhattacharjee S. DLS and zeta potential – what they are and what they are not? J Control Release. 2016;235:337–351.
30. Zhang Y, Huo M, Zhou J, et al. DDSolver: an add-in program for modeling and comparison of drug dissolution profiles. AAPS J. 2010;12(3):263–271.
31. Costa P, Lobo JMS. Modeling and comparison of dissolution profiles. Eur J Pharm Sci. 2001;13(2):123–133.
32. ICH. Q1A(R2): Stability Testing of New Drug Substances and Products. International Council for Harmonisation; 2003.
33. Shegokar R, Müller RH. Nanocrystals: industrially feasible multifunctional formulation technology for poorly soluble actives. Int J Pharm. 2010;399(1–2):129–139.
34. Peltonen L, Hirvonen J. Pharmaceutical nanocrystals by nanomilling: critical process parameters, particle fracturing and stabilization methods. J Pharm Pharmacol. 2010;62(11):1569–1579.
35. Lee J, Choi JY, Park CH. Characteristics of polymers enabling nano-comminution of water-insoluble drugs. Int J Pharm. 2008;355(1–2):328–336.
36. Tuomela A, Hirvonen J, Peltonen L. Stabilizing agents for drug nanocrystals: effect on bioavailability. Pharmaceutics. 2016;8(2):16.
37. Bhargav E, Bhargav GC, Reddy YP, Kumar CP, Ramalingam P, Haranath C. A Design of Experiment (DoE) based approach for development and optimization of nanosuspensions of telmisartan, a BCS class II antihypertensive drug. Future J Pharm Sci. 2020. doi:10.1186/s43094-020-00032-2.
38. Danaei M, Dehghankhold M, Ataei S, et al. Impact of particle size and polydispersity index on the clinical applications of lipidic nanocarrier systems. Pharmaceutics. 2018;10(2):57.
39. Wu L, Zhang J, Watanabe W. Physical and chemical stability of drug nanoparticles. Adv Drug Deliv Rev. 2011;63(6):456–469.
40. Noyes AA, Whitney WR. The rate of solution of solid substances in their own solutions. J Am Chem Soc. 1897;19(12):930–934.
41. Müller RH, Peters K. Nanosuspensions for the formulation of poorly soluble drugs: I. Preparation by a size-reduction technique. Int J Pharm. 1998;160(2):229–237.
42. Kesisoglou F, Panmai S, Wu Y. Nanosizing – oral formulation development and biopharmaceutical evaluation. Adv Drug Deliv Rev. 2007;59(7):631–644.
43. Korsmeyer RW, Gurny R, Doelker E, Buri P, Peppas NA. Mechanisms of solute release from porous hydrophilic polymers. Int J Pharm. 1983;15(1):25–35.
44. Peppas NA, Sahlin JJ. A simple equation for the description of solute release. III. Coupling of diffusion and relaxation. Int J Pharm. 1989;57(2):169–172.
45. Higuchi T. Mechanism of sustained-action medication: theoretical analysis of rate of release of solid drugs dispersed in solid matrices. J Pharm Sci. 1963;52(12):1145–1149.
46. Verma S, Gokhale R, Burgess DJ. A comparative study of top-down and bottom-up approaches for the preparation of micro/nanosuspensions. Int J Pharm. 2009;380(1–2):216–222.